International Journal of Advanced Technology and Engineering Exploration, Vol 12(125)
ISSN (Print): 2394-5443 ISSN (Online): 2394-7454
http://dx.doi.org/10.19101/IJATEE.2024.111100206

Research Article

Optimized fuzzy c-means clustering for liver segmentation using Jaccard-interpolated tuna swarm algorithm

S. Subha[1*] and U. Kumaran[2]
Research Scholar, Department of Computer Applications, Noorul Islam Centre for Higher Education, Noorul Islam University, Thuckalay, Kanyakumari, Tamilnadu, India[1]
Associate Professor, Department of Artificial Intelligence and Data Science, Saveetha Engineering College, Thandalam, Chennai, Tamilnadu, India[2]

Received: 24-February-2024; Revised: 15-April-2025; Accepted: 18-April-2025

Abstract
Accurate liver segmentation from CT images is essential for diagnosis, treatment planning, and surgical interventions in hepatic diseases. Manual segmentation is time-consuming and subject to inter-observer variability, necessitating efficient automated solutions. This study proposes a novel liver segmentation approach based on the Jaccard with interpolation scaled tuna swarm-based fuzzy c-means (JISTS-FCM) clustering algorithm. The methodology comprises four primary stages: pre-processing, feature extraction, clustering, and bounding box generation. Pre-processing enhances CT images using Z-score normalization, contrast enhancement through covariianced contrast limited adaptive histogram equalization (CCLAHE), and noise reduction via the edge preserved median filter (EPMF). Feature extraction is performed using the local tetra pattern (LTP) and adaptive edge detectors. For segmentation, the proposed JISTS-FCM algorithm integrates the tuna swarm optimization (TSO) to improve cluster initialization, replaces Euclidean distance with the Jaccard similarity measure, and incorporates interpolation scaling to enhance convergence and segmentation precision. The random walker method is then used to construct accurate bounding boxes around the segmented liver regions. The method is validated on the 3D-IRCADb dataset, achieving superior performance with a dice similarity coefficient (DSC) of 97.55%, outperforming baseline methods including traditional FCM and cuckoo search algorithm (CSA)-FCM. Additional metrics such as Jaccard similarity coefficient (JSC), volumetric overlap error (VOE), average symmetric surface distance (ASSD), relative volume difference (RVD), and root mean square symmetric surface distance (RMSSD) further confirm the accuracy and robustness of the proposed method. The results demonstrate that JISTS-FCM effectively addresses over-segmentation, irregular boundary delineation, and computational inefficiencies, providing a reliable and automated liver segmentation framework for clinical applications.

Keywords
Liver segmentation, Fuzzy c-means clustering, Tuna swarm optimization, Jaccard similarity, Medical image processing, Computed tomography.

1.Introduction
Certain severe disorders, such as liver disease, pose significant threats to human health and survival. Liver tumors are currently the second leading cause of mortality in males and the sixth leading cause of death in females [1, 2]. The prognosis for liver cancer remains poor. Only 5–15% of patients are eligible for surgical liver resection, which is typically feasible only in early-stage cases with sufficient hepatic regenerative capacity and minimal cirrhosis. Furthermore, right hepatectomy is associated with a higher risk of postoperative complications compared to left hepatectomy [3].

Computed tomography (CT) imaging is commonly employed in the diagnosis and surgical planning of abdominal diseases and is particularly effective for identifying liver conditions, including hepatocellular carcinoma [4, 5]. Liver resection procedures rely heavily on interpolated CT imaging for tasks such as volume estimation, radiation therapy planning, and liver transplantation [6–8]. However, manual segmentation of the liver in individual CT slices is labor-intensive, time-consuming, and prone to

*Author for correspondence

inconsistency, thereby highlighting the need for fully automated liver segmentation methods to expedite diagnosis, monitoring, and treatment planning [9].

Semantic segmentation, a major research area in computer vision, involves labeling each pixel in an image to distinguish different structures. This technique is essential in domains such as autonomous driving and augmented reality [10]. Despite advances in artificial intelligence (AI) and deep learning, liver segmentation from abdominal CT images remains a challenge due to complex anatomical structures, scale variation, and ambiguous boundaries [11]. Conventional vascular segmentation methods—such as model-based tracking, least-cost path algorithms, and active contour models—often fail to accurately segment small vessels and blurred borders [12]. Recent developments in deep learning, including attention-guided networks [13], cascaded incremental learning models [14], and convolutional neural networks (CNNs) [15], have shown promising improvements in segmentation accuracy.

Despite considerable advancements in the field of medical image analysis, liver segmentation remains a technically challenging task due to several unresolved issues. One of the primary concerns is over-segmentation, where current algorithms inaccurately delineate boundaries, often including adjacent anatomical structures or artifacts [16, 17]. Moreover, normal CT images frequently lack sufficient contrast or feature richness, which leads to mis-segmentation of liver regions and tumors, particularly in cases with low contrast variation or diffuse boundaries [18]. Traditional segmentation approaches that rely on texture-based features, such as the gray level co-occurrence matrix (GLCM), are often inadequate for capturing intricate liver edges and internal tumor details, thereby limiting their applicability in clinical scenarios [19]. Furthermore, conventional clustering techniques, including fuzzy c-means (FCM), exhibit poor performance when dealing with irregular, non-linear liver shapes and complex tissue heterogeneities, especially in the presence of pathological anomalies such as tumors or fibrotic textures [20]. These challenges necessitate the development of more robust, adaptive, and optimization-driven segmentation frameworks.

The primary aim of this study is to develop an advanced, optimization-based liver segmentation approach capable of overcoming limitations in existing methods. Specifically, the objectives are to: (1) address the prevalent issues of over-segmentation and mis-segmentation through an improved clustering strategy; (2) implement the Jaccard with interpolation scaled tuna swarm-based fuzzy c-means (JISTS-FCM) clustering algorithm to improve the accuracy of segmentation boundaries; (3) integrate the Random Walker method for precise construction of liver bounding boxes to enhance localization; and (4) apply robust pre-processing and enhancement techniques to improve image quality and segmentation precision.

This research makes several key contributions to the domain of medical image segmentation. Firstly, it proposes a novel JISTS-FCM framework, which leverages the tuna swarm optimization (TSO) strategy and Jaccard similarity-based interpolation scaling to improve the convergence and clustering accuracy of the FCM algorithm. Secondly, it addresses critical segmentation challenges such as boundary ambiguity and low-contrast feature separation, particularly in heterogeneous liver tissues. Thirdly, the study incorporates the random walker algorithm for refining the spatial delineation of liver boundaries, thereby ensuring geometrical consistency. Lastly, a comprehensive performance evaluation is conducted using 3D-IRCADb dataset, validating the proposed method's superiority over existing techniques in terms of segmentation accuracy, robustness, and computational efficiency.

The research that has been provided is organized in the following way: section 2 explains the recent reviews; section 3 describes the suggested portion; section 4 conducts an experimental study of the proposed research; and section 5 concludes the article with future improvements.

2.Literature review

Numerous automated liver segmentation strategies have been proposed, including texture-based strategies, statistical shape models, region growing and threshold strategies, graph cut strategies, and sigmoid edge strategies. However, these approaches often suffer from inadequate feature representation and heavily rely on handcrafted features, limiting their effectiveness. Recent advancements have seen the development of deep learning models for more accurate segmentation. Budak et al. [21] introduced a cascaded deep convolutional encoder-decoder neural network (EDCNN) for effective liver tumor segmentation (LiTS). In their approach, an initial EDCNN is trained to segment the liver from CT scans, and a second EDCNN subsequently segments the tumor sites within the liver regions of interest

(ROIs) identified by the first network. This cascading method allows for improved segmentation accuracy with a minimal number of training images. Li et al. [22] proposed an approach for accurate liver segmentation from CT scans, which addressed issues such as intensity variations and pathological changes. The method combines a level set model with intensity bias and position constraints, followed by a sparse shape composition (SSC) technique and enhanced graph cut to improve segmentation outcomes.

Alalwan et al. [23] investigated the performance of the DenseUNet-569 model, a 3 Dimensional (3D) deep learning network designed for semantic segmentation of liver and tumor sections. DenseUNet-569 features depth-separable convolution (DS-Conv), replacing traditional convolution layers to significantly reduce computational costs and graphics processing unit (GPU) memory requirements. This architecture results in better performance for 3D liver and tumor segmentation due to its deep network structure and efficient parameter utilization. Aghamohammadi et al. [24] enhanced liver and tumor segmentation in CT images by tackling issues like unclear boundaries and irregular shapes. A cascade CNN is used, with Z-Score normalization and a new local direction of gradient (LDOG) encoding algorithm to highlight key image features, particularly near the liver's edge. By opting for a straightforward CNN model, the method reduces training and testing times while delivering higher accuracy and efficiency compared to other state-of-the-art approaches.

Ahmad et al. [25] develop an efficient method for liver segmentation in CT images, addressing the limitations of existing deep learning approaches that require extensive training time and hardware resources. Additionally, the proposed lightweight gaussian-weight initialization of convolutional neural network (Ga-CNN) features three convolutional and two fully connected layers, utilizing softmax for liver-background discrimination and random Gaussian distribution for weight initialization. Experiments on benchmark datasets, including MICCAI SLiver’07, 3Dircadb01, and LiTS17, demonstrate that the Ga-CNN effectively extracts liver regions with strong performance across all datasets. Fan et al. [26] enhanced the accuracy of liver and tumor segmentation by introducing a new network, Multi-scale Attention Net (MA-Net), which leverages self-attEention mechanisms to integrate local and global features. Additionally. the network incorporates two key blocks: the position-wise attention block (PAB) for capturing spatial dependencies, and the multi-scale fusion attention block (MFAB) for fusing multi-scale semantic features across channels. Tested on the MICCAI 2017 LiTS dataset, MA-Net achieves superior segmentation performance, with dice scores of 0.960 for the liver and 0.749 for tumors.

Alirr [27] developed an automatic method for liver and tumor segmentation from CT scans to assist in hepatic surgical planning. The method employs a fully convolutional neural network (FCNN) combined with a region-based level set function. Initially, the fully convolutional network (FCN) predicts a coarse segmentation of the liver and tumors, which is then refined by the region-based level set to achieve accurate results. The approach was validated using the LiTS and IRCAD datasets, achieving Dice scores of 95.6% and 70% for liver and tumor segmentation in LiTS, and 95.2% and 76.1% in IRCAD, demonstrating its effectiveness in clinical applications.

Tang et al. [28] introduced a pioneering two-stage model named deep supervised learning (DSL), employing faster region based convolutional neural network (R-CNN) for initial liver detection and DeepLab for precise contour refinement. Building on this, Rahman et al. [29] proposed the ResUNet model, a hybrid architecture combining the strengths of ResNet and UNet, tailored for efficient segmentation of liver and tumors using CT volumes from IRCADB01. Kushnure and Talbar [30] addressed the limitations of fixed geometric structures in convolutional kernels and spatial context loss in deep networks by adopting a multi-scale approach. Their method enhanced CNN's receptive field, extracting both global and local features more granularly through channel-wise recalibration of aggregated multi-scale features. Similarly, Winkel et al. [31] evaluated an AI-based software for liver volumetric analysis, demonstrating its efficacy against manual segmentation across 462 multiphasic CT datasets. The software leveraged multi-scale deep-reinforcement learning for 3D marker detection and structure segmentation, contributing to improved accuracy in liver volume assessment. Almotairi et al. [32] repurposed SegNet, originally designed for road scene classification, to tackle liver CT segmentation challenges. SegNet, a deep convolutional encoder-decoder architecture, proved effective in handling complex liver and tumor boundaries with hierarchical feature extraction layers. Tang et al. [33] explored the

application of CNNs in selective internal radiation therapy (SIRT) for automating liver segmentation, aiming to reduce variability among observers. Their CNN model, trained and validated on diverse datasets including SIRT patient data and challenge datasets, demonstrated robust performance in segmenting liver structures from CT images. Ranjbarzadeh and Saadi [34] introduced a novel method focusing on automated liver and tumor segmentation. Their approach integrated edge extraction via the Kirsch filter, concave and convex point (CCP) calculations, and mean-shift algorithm for enhancing image uniformity along organ borders. Utilizing FCM for segmentation, their method aimed to improve diagnostic accuracy in liver diseases through fully automated computer-aided software. In 2021, Lei et al. [35] proposed Deformable Encoder-Decoder Network (DefED-Net), a DefED-Net tailored for CT image segmentation. Incorporating deformable convolutions for adaptive kernel learning and a ladder-atrous-spatial-pyramid-pooling module for enhanced context learning, DefED-Net aimed to address challenges such as irregular shapes and spatial context loss, further advancing the state-of-the-art in liver and tumor segmentation from medical images. These advancements collectively highlight the growing effectiveness and versatility of deep learning approaches in transforming the diagnosis and treatment planning of hepatic diseases through automated image analysis.

3.Methods

Liver segmentation using CT scans is a critical step in the automated identification of liver tumors and vessels, 3D visualization, and various planning stages for interventional surgeries, including multiphase registration and automated route planning. Given that the time available for surgical planning is often limited to just a few minutes, manual delineation of the liver boundaries in each CT slice becomes both time-consuming and impractical. Consequently, there is a strong need for fast and accurate liver segmentation in clinical environments. To address this challenge, the present study introduces an efficient liver segmentation methodology based on the JISTS-FCM algorithm. The block diagram of the proposed methodology is illustrated in *Figure 1*. This approach comprises four main stages, which are described in detail below.

3.1Pre-processing

Pre-processing is carried out through three main stages: normalization, contrast enhancement, and filtering. *Figure 2* illustrates the CT image before and after the application of the edge preserved median filter (EPMF), demonstrating the effectiveness of the preprocessing steps in enhancing image quality.

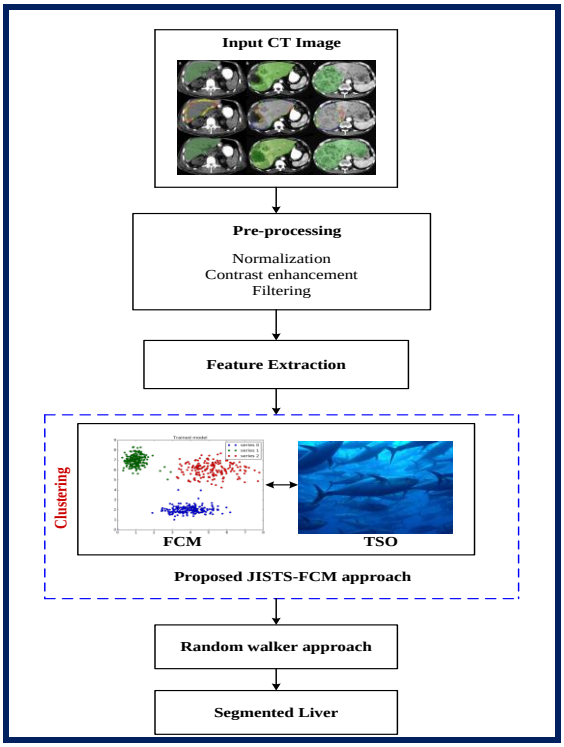

Figure 1 Block diagram for the proposed research methodology

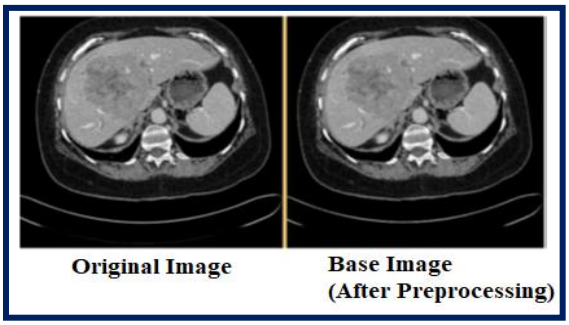

Figure 2 Before and after image preprocessing with edge preserved median filter

Normalization

Normalization using the Z-score has been applied in this study, enhancing the distinction between the liver and tumor in the resulting image. The Z-score normalization transforms the range of pixel intensity values linearly, ensuring a mean of 0 and a variance of 1. To compute the Z-score, the mean pixel intensity values are subtracted from the original pixel values, aligning the mean with zero. The result is then divided by the standard deviation to balance the

spread of the data, as outlined in [36]. The normalization process, based on the Z-score, is mathematically represented by Equation 1.

$$ZS = \frac{w_i - \lambda}{\sigma} \quad (1)$$

Where, ZS are the normalized values for the z-score. λ, σ the mean and standard deviation of the data values, w_i as well as the original values. Then, using a liver mask to remove non-liver information, lower the noise, and combine complicated histograms of tumors in various situations, Z-score normalization and an anisotropic diffusion filter were employed.

Here, ZS represents the normalized values obtained using the Z-score. In this expression, λ and σ denote the mean and standard deviation of the data values, respectively, while w_i refers to the original pixel intensity values. To enhance liver region clarity, a liver mask was applied to eliminate non-liver regions, reduce noise, and merge complex tumor histograms across varying conditions. This was achieved by employing Z-score normalization in conjunction with an anisotropic diffusion filter.

Contrast enhancement

The contrast level is increased to extract more information from the picture, and the process of contrast enhancement also addresses the issue of blurring borders. The covarianced contrast limited adaptive histogram equalization (CCLAHE) algorithm is used in this suggested technique. Here, the adaptive histogram equalization approach may be used to enhance the quality of medical pictures gathered using various modalities, leading to better segmentation at a later stage. As adaptive histogram equalisation for CT images makes them excessively bright to see, CLAHE was used in this experiment to address the over-amplification problem. The clip limit is set at 4 and the total tile size is 8 for the CCLAHE implementation.

Filtering

The CT image often contains a variety of noises that might compromise the quality of the segmentation. Therefore, this suggested approach applies an EPMF to filter the input picture. Grey-scale photos with noise are cleaned up by the EPMF. Edges are thought to be an important indicator of lung illness. To ameliorate the weak edge preservation conditions of the median filter, the edge halting function is taken into account as a filter parameter. The EPMF is used to perform the noise reduction process for the resulting greyscale pictures. The representation of the grayscale image is Δ_g^n. By replacing a pixel's value with the median of its nearby pixel values, the median filter lowers noise. The neighborhood of the centre pixel is used to get the median value, and the median filtering is given in Equation 2.

$$\Delta_g^n = ES\left[\eta\left(\Delta_g^n(x,y)\right)\right] \quad (2)$$

The output of the noise-removed image is denoted by η, which represents the median value of each pixel after the filtering process. The edge-stopping function is represented by Ψ, as defined in Equation 3.

$$\Psi = \frac{1}{(1+(d|\eta(x,y)|U)^2)} \quad (3)$$

The parameter that determines the amount of diffusion needed to preserve the edges is shown, and it is based on the rate of diffusion around the edges. Using the CCLAHE approach, the contrast of the noise-removed image (Δ_{NR}^n) is improved, and the final contrast-enhanced image is represented by (Δ_{CE}^n).

3.2Feature extraction

The process of segmentation is crucial for the segmentation of the liver. The supplied input picture is divided into many pieces using segmentation. After pre-processing, form characteristics, texture, such as the local tetra pattern (LTP), and edge features utilizing a clever edge detector are retrieved [37]. LTP extracts information based on the distribution of coded edges in two directions (positive or negative direction). The ability to split edges in more than two directions can be improved.

Algorithm

Input: Query image

Output: Retrieval result

1. Look at the image and make it grayscale.
2. Use the first order derivatives of the horizontal and vertical axes.
3. Determine the direction of each pixel.
4. Use the first order derivatives of the horizontal and vertical axes.
5. Divide the four models into three binary models based on your calculations.

3.3Jaccard with interpolation scaled tuna swarm based fuzzy c-means clustering algorithm

Based on the extracted features, liver boundary segmentation is performed using the proposed JISTS-FCM algorithm. Traditional FCM methods often rely on random centroid initialization, which can lead to inaccurate clustering results. To address this issue, the proposed methodology incorporates TSO for optimal centroid selection. Within the TSO

framework, a control strategy is employed to enhance convergence reliability. To further improve accuracy, the strategy integrates an interpolation-based scaling factor. Additionally, the conventional use of Euclidean distance in FCM is not ideal for large datasets or non-Euclidean feature spaces. Therefore, the proposed method replaces Euclidean distance with a more robust similarity measure—specifically, the Jaccard similarity—and utilizes Manhattan distance to better capture the dissimilarity in high-dimensional data. The cluster formation in the proposed approach is designed to minimize the objective function (OF), as defined in Equation 4.

$$OF = \sum\sum D_{xy}^{R} L_{xy} \quad (4)$$

Where, R is any real integer higher, $L_{xy}$is the distance between nodes, and$x$ is the degree of cluster membership for each node D_{xy}^{R}. Calculating the standard deviation between nodes, which is represented as follows, first determines the centroid point per Equation 5.

Here, R is a real-valued exponent, L_{xy} represents the distance between nodes x and y, and D_{xy}^{R} denotes the degree of cluster membership for each node. The centroid point is determined by first calculating the standard deviation between nodes, as shown in Equation 5.

$$Q_i = \sqrt{\frac{\sum \alpha_S - \mu}{\alpha_n}} \quad (5)$$

Where, Q_i specifies the cluster centre, and μ indicates the mean value. After the calculation of centre vector, the distance matrix is calculated based on Manhattan distance calculation this is given as follows in Equation 6.

$$L_{xy} = |Q_{i+1} - Q_i| + |\alpha_{i+1} - \alpha_i| \quad (6)$$

Then, update the partition matrix for the j^{th} step is derived as follows in Equation 7.

$$D_{xy}^{R} = \left(1 \Big/ \sum \left(L_{xy} / L_{sy} \right)^{2/R-1} \right) \quad (7)$$

Where, s denotes the iteration step. The FCM process is repeated until it converges. In this way the cluster is formed. The formed cluster is denoted as shown in Equation 8.

$$H_S = \{h_1, h_2, h_3, \ldots . h_n\} \quad \text{(or)} \quad H_S = h_i, i = 1,2, \ldots . , n \quad (8)$$

Where, H_S indicates the formed cluster sets and h_n defines the n-number of clusters.

This variable may be selected based on the size of the supplied picture. To eliminate boundaries that were created randomly, the adjacent tiles are then blended using the Jaccard algorithm with scaled interpolation. To avoid highlighting any extraneous material in photographs, such as noise, the contrast may be lowered, particularly in homogenous areas. Here, the liver was divided using the Jaccard method with scaled interpolation. The marine carnivorous fish behavior, which is to be the strongest in every generation, served as the basis for the development of the tuna optimization algorithm. Spiral foraging and parabolic foraging, two distinctive foraging behaviours, are used to hunt for the best answer. However, it has a local optimum issue for complicated data, which might make its already subpar searching much worse. This research approach sometimes uses a control strategy that uses Jaccard with interpolation scaled to address that issue. The suggested approach offers a rapid convergence rate global search. Each cluster's liver segmentation in this case is referred to as a tuna swarm. The TSO algorithm initiates the optimization process by uniformly generating an initial population at random within the search space, similar to other swarm-based meta-heuristic algorithms, as defined in Equation 9.

$$Z_j^{\text{int}} = R.(ub - lb) + lb, \quad i = 1,2,\ldots,NP, \quad (9)$$

Where X_j^{int} is the j^{th}first individual, ub and lb represent are the higher and lower search space boundaries. R represents a uniformly distributed random vector with values between 0 and 1, where NP is the total number of tuna populations.

Spiral Foraging

To avoid being caught by predators, sardines, sardines, and other small fish constantly change their swimming direction upon contact. The school of tuna now forms a compact spiral pattern to follow its prey [38]. When a small group of fish swims steadily in one direction, nearby fish gradually adjust their course and eventually form a larger group with the same objective. Most of the fish in the school follow this movement, even if they are not strong enough to lead on their own. Schools of tuna not only follow food but also communicate with each other. Each tuna follows the fish in front of it, allowing communication between tunas in the area. Based on the above concepts, the mathematical equation to find spiral feed per Equation 10 to Equation 14.

$$Z_j^{n+1} = \begin{cases} \alpha_1.(Z_{best}^n + \beta.\left|Z_{best}^n - Z_j^n\right|) + \alpha_2.Z_j^n i=1, \\ \alpha_1.(Z_{best}^n + \beta.\left|Z_{best}^n - Z_j^n\right|) + \alpha_2.Z_{j-1}^n i=2,3,\ldots,NPM, \end{cases} \quad (10)$$

$$\alpha_1 = x + (1-x).\frac{n}{n_{max}}, \quad (11)$$

$$\alpha_2 = (1-x) - (1-x).\frac{n}{n_{max}} \quad (12)$$

$$\beta = e^{ck}.cos(2\pi c), \quad (13)$$

$$k = e^{3\,cos(((n\frac{1}{n_{max}}} \quad (14)$$

Where Z_j^{n+1} is the j^{th}iteration's$n+1$ individual, $Z_{best}^n$is the current ideal person (food), and $\alpha_1$and$\alpha_2$are the weight coefficients that control the probability it is for people to go in the direction of the ideal individual and the previous individual, In the first step, x is a constant used to measure how well tuna follows the ideal person and the previous person, and n is an integer that is equally divided between 0 and 1.

When spiral foraging, all tunas have an excellent ability to use the vicinity of the feeder as a foraging area. However, blindly following an individual foraging when food is not available for a suitable individual does not promote social foraging. For this reason, a spiral search is initiated from a randomly generated location in the search space. It is now easier for individuals to explore a large area, and TSO is now ready to conduct global explorations. The characteristics of the proposed mathematical model are defined as shown in Equation 15.

$$Z_j^{n+1} = \begin{cases} \alpha_1.(Z_R^n + \beta.\left|Z_R^n - Z_j^n\right|) + \alpha_2.Z_j^n, j=1, \\ \alpha_1.(Z_R^n + \beta.\left|Z_R^n - Z_j^n\right|) + \alpha_2.Z_{j-1}^n, j=2,3,..,NP, \end{cases} \quad (15)$$

WhereX_R^n in the search space is a reference point that was randomly chosen.

For example, meta-heuristic algorithms often start with global deep mining before gradually moving to concentrated local mining. Therefore, as the number of iterations increases, the reference point of the TSO spiral regime changes from random individuals to optimal individuals. The final mathematical model of the spiral feeding strategy is summarized in Equation 16.

$$Z_j^{n+1} = \begin{cases} \{ \alpha_1.(Z_R^n + \beta.\left|Z_R^n - Z_j^n\right|) + \alpha_2.Z_j^n, j=1 \\ \alpha_1.(Z_R^n + \beta.\left|Z_R^n - Z_j^n\right|) + \alpha_2.Z_{j-1}^n, j=2,3,\ldots,NP, if R < \frac{n}{n_{max}} \\ \{ \alpha_1.(Z_{best}^n + \beta.\left|Z_{best}^n - Z_j^n\right|) + \alpha_2.Z_j^n, j=1 \\ \alpha_1.(Z_{best}^n + \beta.\left|Z_{best}^n - Z_j^n\right|) + \alpha_2.Z_{j-1}^n, \mathbb{N} j=2,3,\ldots,NP, if R \geq \frac{n}{n_{max}} \{ \end{cases} \quad (16)$$

Parabolic Foraging

Tunas work together to find food by making both a circle and a circular pattern. Tuna forms a parabola shape by using food as a point of reference. Additionally, tuna search for food by looking everywhere [39]. Both methods are used simultaneously, with each having a 50% chance of being chosen. The mathematical model is detailed in Equations 1) and 18.

$$Z_j^{n+1} = \begin{cases} Z_{best}^n + R.(Z_{best}^n - Z_j^n) + RN.M^2.(Z_{best}^n - Z_j^n), if R < 0.5 \\ RN.M^2.Z_j^n, if R \geq 0.5, \end{cases} \quad (17)$$

$$M = (1 - \frac{n}{n_{max}\frac{n}{n_{max}}} \quad (18)$$

RN is an arbitrary number that may have a value of 1 or -1.

Prior to locating prey, tuna use two foraging strategies in cooperative hunting. The population chooses to update its position in the search space based on probability z, or the TSO first randomly chooses which of the two forging approaches to use in the optimization. The value of parameter z is covered by the simulation tests of the parameterization. Throughout the optimization process, all TSO characters are continuously updated and computed until the final state is reached. At this point, the corresponding trait and the corresponding fitness value are returned. *Figure 3* shows the present the organizational flowchart of the Tuna Swarm Optimization Algorithm integrated with-Fuzzy C-means (TSO-FCM).

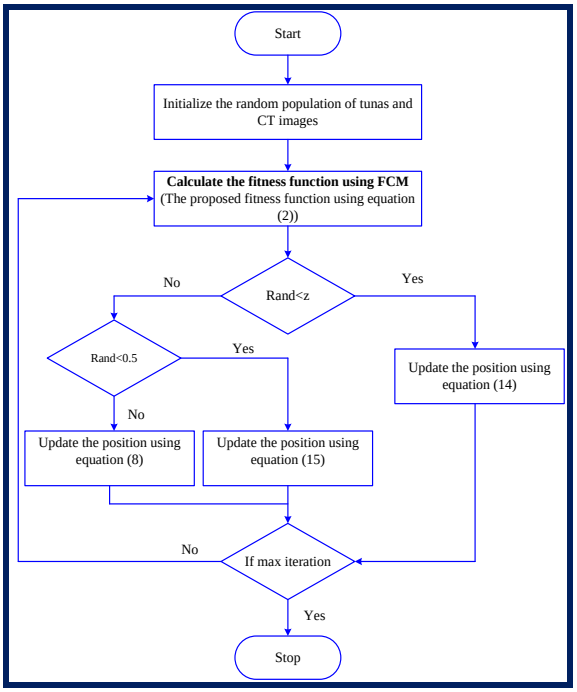

Figure 3 Flowchart of proposed TSO-FCM

When tuna work together to hunt, they use two different ways to find food before they find their target. The populations first pick at random which of the two hunting methods to use in the TSO optimisation process, or they choose to start over at a different point in the search space based on a chance of z. This experiment will look at the value of parameter z as it sets up the scenario. During the optimisation process, all TSO people are constantly updated and calculated until the end condition is met. At this point, the optimal solution and its corresponding fitness value are returned. *Figure 3* illustrates the sequence of the proposed (TSO-FCM).

3.4Random walker method

The number of random walks is adjusted depending on the pre-segmented slices in order to greatly minimize computation time without sacrificing the quality of the output. Since they compete directly with the random walks of the neighbouring label, the random walks close to the object's edges are critical for high-quality segmentation. Random walks that begin deep within the object have little chance of winning against other random walks [40]. In order to speed up the computation, fewer random walks are performed in the inner region. The random walker approach is utilized to create the hepatic region's bounding box. The input picture is produced as a graph in this approach, which may be represented as $G = (U, V)$. Here, u∈U represents a pixel corresponding to a node in the graph, while u∈U also denotes the set of edges where neighboring pixels are connected.

Procedure of RW algorithm

Step 1: Weight calculation

Each edge's weight indicates the likelihood that a random walker will be mitigated by that edge. The segmentation qualities are evaluated using the following weight value based on the rule of minima (Equation 19).

$$Wt_{xy} = L_{xy} * min\left(\frac{\theta}{\pi}, 1\right) \quad (19)$$

Here,θ represents the external dihedral angle across the edge and L_{xy}means the edge length between pixels x and y.

Step 2: Graph calculation

The graph's Laplacian matrix is then calculated as follows in Equation 20.

$$LP_{xy} = \begin{cases} d_x & if\ x = y \\ -W_{xy} & if u_x is neighbor to u_y \\ 0 & otherwise \end{cases} \quad (20)$$

Here, d_x represents the pixel u's degree and is defined as follows in Equation 21.

$$d_u = \sum_{k \in S_u} w_{uk} \quad (21)$$

Here, *du* represents the collection of pixels that are near u. The nodes or pixels are divided into two sets, as with$U_i \bigcup U_x = U\ and\ U_i \bigcap U_x = \phi$. The A_U seed nodes, or pixels with known labels, are denoted here U_i, while the unseeded nodes, or pixels with unknown labels, are denoted. Assume that the nodes in L are arranged such that seed nodes are in front of unseeded nodes. Consequently, the Laplacian matrix may be defined as per Equations 22 and 23.

$$LM = \begin{bmatrix} LM_i & Z \\ Z^T & LM_x \end{bmatrix} \quad (22)$$

$Z = (z_{xy})$represents a $k \times n$ matrix in this instance, and it has the following definition.

$$z_{xy} = -\beta D_x \quad (23)$$

β indicates a parameter balancing between the neighbour weights in this context.

Step 3: Selection of segmentation results

The probability isp_x^s represented by when a random walker first arrives at a s labelled seed node from the pixel x. Additionally, the seed nodes represented by the vector $|U_x \times 1|$ and designated with the letter "s" (Equations 24 and 25).

$$g_y^s = \begin{cases} 1 & if\ u_x is labeled as s \\ 0 & if\ u_y is not labeled as s \end{cases} \quad (24)$$

Here,$u_y \in U_i, s \in J and 0 < s \leq K$. By specifying, the answer is calculated for each label s.

$$LM \bigcup y^s = -Z^T g^s \quad (25)$$

The unseeded nodes x may finally be identified as $s = \max_s y_x^s$. Additionally, the labels of the pixels determine how the areas of the pixels are divided. The segmentation result that has been smoothed out is an optional one.

4.Result and discussion

In this section, the performance of the proposed JISTS-FCM approach is evaluated. The implementation of the proposed method was carried out using MATLAB 2021b. The effectiveness of the approach for liver segmentation is assessed using a range of evaluation metrics and is compared against

existing state-of-the-art techniques. Specifically, the performance of the proposed method is analyzed and compared with conventional FCM and the FCM integrated with the cuckoo search algorithm (FCM-CSA) [30].

4.1Dataset explanation

The 3D-IRCADb database was utilized to obtain the experimental images [30]. This dataset includes three distinct tumor types: meningioma, hepatocellular carcinoma, and metastatic carcinoma, comprising a total of 5,646 images. For model development, 70% of the dataset was used for training and the remaining 30% for testing. A five-fold cross-validation strategy was employed to ensure robust performance evaluation. All images were resized to a resolution of 512 × 512 pixels as part of the image enhancement process. Dimensionality reduction was applied to minimize computational complexity and training time without compromising critical diagnostic information. Comparative analysis was conducted by executing each method—JISTS-FCM, CSA-FCM, [41, 42] and traditional FCM—using MATLAB on the 3D-IRCADb dataset. *Figure 4* illustrates the segmentation outcomes: panel (a) shows results from the proposed JISTS-FCM method, while panels (b) and (c) depict the outputs of CSA-FCM and conventional FCM, respectively.

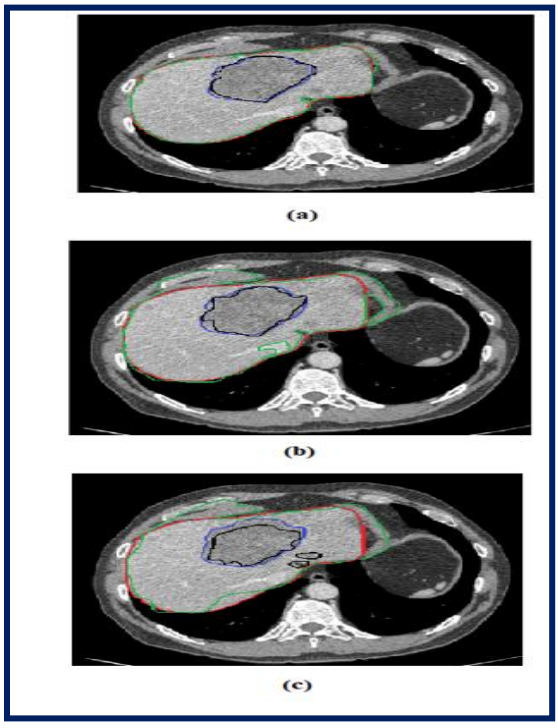

Figure 4 Segmentation results of (a) Proposed scheme (b) CSA-FCM and (c) FCM

4.2Performance metrics

Seven distinct evaluation metrics were used to objectively compare the performance of the proposed method with expert-manually segmented ground truth data. These metrics are widely adopted in state-of-the-art medical image segmentation studies. The primary metric, the dice similarity coefficient (DSC), quantifies the overlap between two binary images and is defined in Equation 26. Additional performance measures are detailed from Equations 27 to 32.

$$\Psi_{DSC} = \frac{2(TP)}{2(TP)+FP+FN} \quad (26)$$

Jaccard similarity coefficient (JSC):

$$\Psi_{JI} = \left|\frac{R \cap S}{R \cup S}\right| \quad (27)$$

Volumetric overlap error (VOE) [%]:

$$\Psi_{VOE} = 100\left(1 - \frac{R \cap S}{R \cup S}\right) \quad (28)$$

Relative volume difference (RVD) [%]:

$$\Psi_{RVD} = 100\left(\frac{|R|-|S|}{|S|}\right) \quad (29)$$

Average symmetric surface distance (ASSD) [mm]

$$\Psi_{ASD} = \frac{1}{|Q(R)|+|Q(S)|}\left(\sum_{Q_R \in Q(R)} d\left(Q_R, Q(S)\right) + \sum_{Q_S \in Q(S)} d\left(Q_S, Q(R)\right)\right) \quad (30)$$

Root mean square symmetric surface distance (RMSSD) [mm]:

$$\Psi_{RMSSD} = \sqrt{\frac{1}{|Q(R)|+|Q(S)|} * \left(\sum_{Q_R \in Q(R)} d^2\left(Q_R, Q(S)\right) + \sum_{Q_S \in Q(S)} d^2\left(Q_S, Q(R)\right)\right)} \quad (31)$$

Maximum symmetric surface distance (MSD) [mm]:

$$\Psi_{MaxD} = Max\left\{\underset{Q_R \in Q(R)}{Max}\, d\left(Q_R, Q(S)\right), \underset{Q_S \in Q(S)}{Max}\, d\left(Q_S, Q(R)\right)\right\} \quad (32)$$

True positive (TP) in the DSC measure denotes that the observed value and anticipated value are both 1. False positive (FP) refers to a situation in which the expected value is 1 but the actual value is 0. FP is the opposite of TP, when the observed value is 1 but the expected value is 0.

In the last five measures, R represents the segmented volume created by the suggested approach, $Q(R)$ signifies the collection of surface voxels R, and $S$is the ground truth. A voxel's V shortest distance

from to $Q(R)$ is given by $d(V, Q(R)) = Min_{Q_R \in Q(R)} \|V - Q_R\|$ where $\|\cdot\|$ is the Euclidean distance. For a perfect segmentation, DSC is 1 and all other indicators are 0.

Table 1 presents a comprehensive comparative analysis of the proposed JISTS-FCM method against conventional segmentation techniques—namely FCM and CSA-FCM—using key evaluation metrics such as DSC, VOE, JSC, RVD, ASSD, MSD, and RMSD. As illustrated in *Figure 5*, the proposed method outperformed both FCM and CSA-FCM, achieving superior accuracy and overlap with ground truth annotations. Specifically, the success rates of FCM, CSA-FCM, and the proposed JISTS-FCM were 83%, 92%, and 97.86%, respectively. Sensitivity and specificity values for the proposed method were 96.15% and 95.75%, respectively, confirming its robustness in accurately segmenting liver regions.

Figure 6 highlights the computational complexity of the methods. The average processing times for JISTS-FCM, CSA-FCM, and FCM were 0.9812, 2.4561, and 3.2945 seconds, respectively, indicating that the proposed method is not only more accurate but also more efficient. These results underscore the proposed algorithm's potential for real-time clinical applications. Further qualitative results, shown in

Figure 4, demonstrate the segmentation quality of the proposed method in comparison to CSA-FCM and traditional FCM. These visual outputs validate JISTS-FCM's capability in accurately identifying liver boundaries and tumor regions, which is critical in medical diagnostics. Receiver operating characteristic (ROC) analysis in *Figure 7* shows an area under the curve (AUC) of 0.92 for the proposed method, reflecting high classification performance. Compared to traditional FCM, which achieved a slightly lower AUC (>0.90), JISTS-FCM exhibited greater precision in evaluating liver segmentation outcomes. *Figure 8* presents confusion matrices for three tumor types, further supporting the model's diagnostic effectiveness.

Table 2 compares the performance of the proposed method with several state-of-the-art liver segmentation techniques reported in recent literature. The JISTS-FCM approach achieved a DSC of 97.55%, outperforming methods such as random walker [43] and V-Net and Wasserstein GAN-based model [VNet-WGAN] [44], both of which achieved a DSC of 94.03%. On datasets such as SLiver'07 and 3D-IRCADb, the proposed method consistently delivered superior results.

Table 3 presents a comparative analysis based on VOE, RVD, and ASSD. The proposed method achieved the lowest VOE (1.341%), outperforming Laplacian mesh optimization (LMO) (4.9%) [45], Multiphase contrast-enhanced FCM (6.2%) [46], and other deep learning approaches like Edge enhancement based Densely connected convolutional neural network and console commend processor [CCP]. These findings highlight the method's precision and adaptability in accurately segmenting liver tissues, even under complex imaging conditions.

The JISTS-FCM methodology demonstrated clear superiority across all evaluated metrics. Its integration of optimization, similarity-based clustering, and probabilistic region delineation allows for accurate, efficient, and scalable liver segmentation, making it a strong candidate for adoption in clinical and research settings.

Table 1 The performance analysis of the proposed scheme in terms of DSC, VOE, JSC, RVD, ASSD, MSD and RMSD

Test images	DSC (%)	VOE (%)	JSC (%)	RVD (%)	ASSD (mm)	MSD (mm)	RMSD (mm)
1	94.31	1.723	90.23	0.241	1.342	7.345	1.754
2	95.12	1.590	90.45	0.1843	1.234	7.124	1.741
3	95.42	1.545	91.67	0.1647	1.212	6.812	1.654
4	96.64	1.451	92.67	0.152	1.187	6.354	1.432
5	97.55	1.341	94.23	0.125	1.054	6.124	1.324

Table 2 The comparison with other methods

Method	Test dataset (s)	DSC (%)
Random walker [30]	SLiver'07	94.03
VNET and WGAN [31]	LiTS17	92.00
Multi-scale parallel convolution blocks (MPC) [32]	3D-IRCADb	77.15
Proposed method	3D-IRCADb	97.55

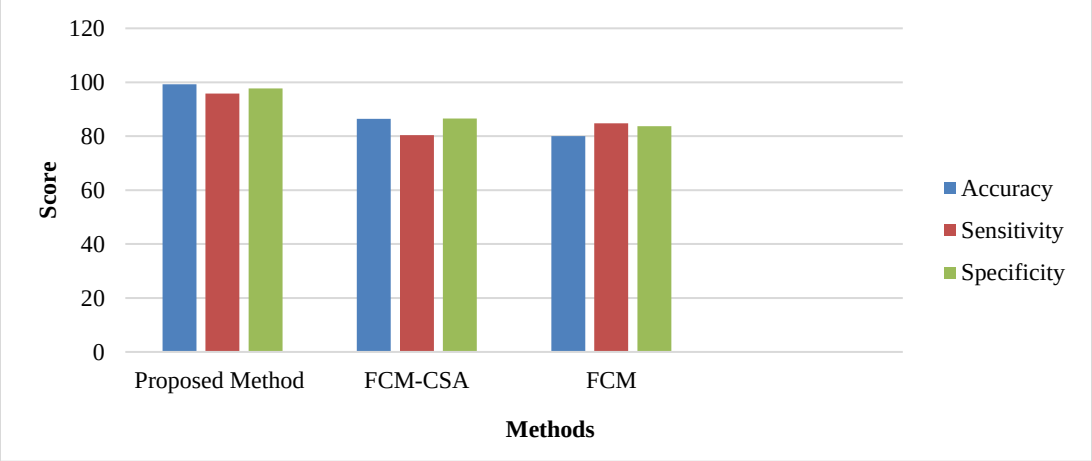

Figure 5 Liver segmentation performance of the proposed and existing methods

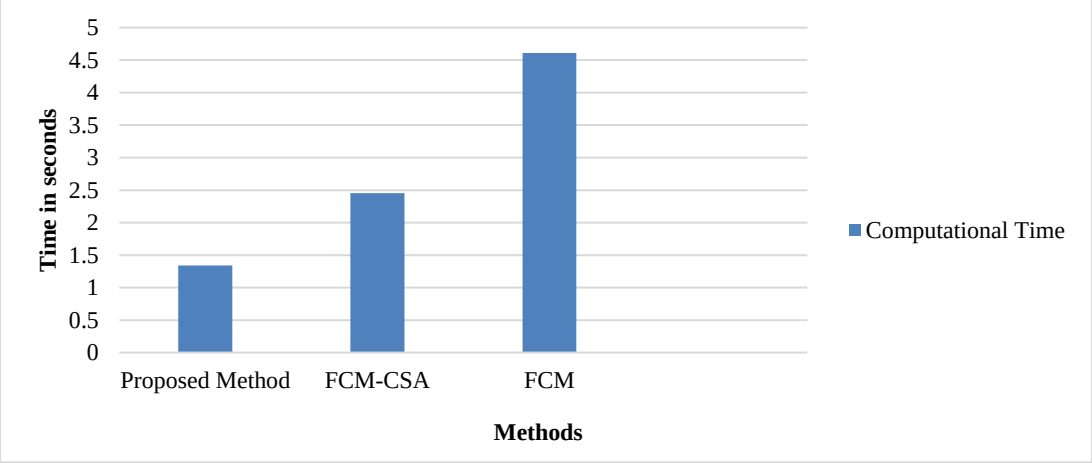

Figure 6 Computational time complexity analysis

Table 3 The comparison of proposed work with the previous work

Ref	VOE (%)	RVD (%)	ASSD (mm)
LMO [33]	4.9	6.7	5.9
Multi-Constraint Fully Convolutional Network (MC-FCN) [34]	6.2	7.3	5.4
EDCNN [16]	4.7	6.7	3.2
CCP [35]	2.9	4.2	2.5
Proposed	1.341	0.125	1.054

This study introduced the JISTS-FCM method for liver segmentation using magnetic resonance imaging (MRI) data from the 3D-IRCADb dataset, and its performance was compared against established methods such as FCM and FCM-CSA. The key findings indicate that JISTS-FCM consistently delivers superior performance across multiple metrics, including DSC, JSC, and ASSD. This superior performance highlights its effectiveness in accurately delineating liver structures from medical images, which is critical for clinical applications such as tumor detection and treatment planning.

The higher DSC and JSC values achieved by the JISTS-FCM method demonstrate better segmentation accuracy and greater overlap with ground truth annotations compared to traditional approaches. This suggests that JISTS-FCM is more reliable for segmenting liver structures, which is essential in clinical settings where precision significantly impacts

diagnostic outcomes. Furthermore, this improved accuracy indicates that the JISTS-FCM method can enhance the quality of medical image analysis, leading to more informed and accurate clinical decision-making.

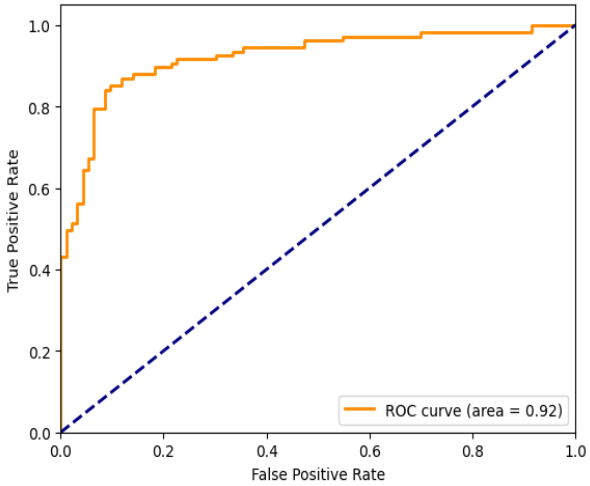

Figure 7 ROC-AUC analysis of proposed approach

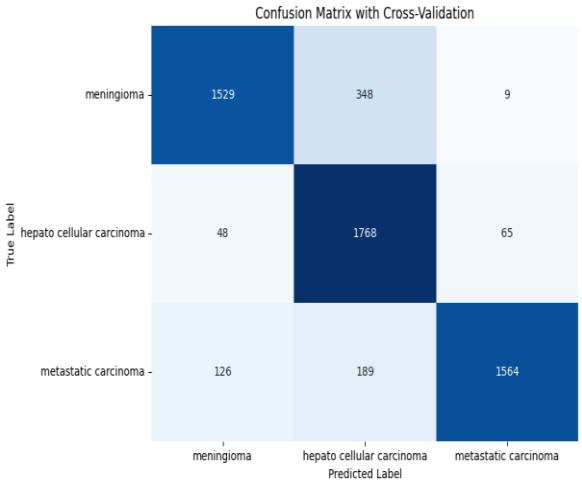

Figure 8 Confusion matrix of the proposed approach

Limitations

The study did find some limitations, though, so it wasn't all sunshine and rainbows. Computing efficiently using the JISTS-FCM method is a big hurdle. Processing times are longer when compared to FCM and FCM-CSA because of the method's higher computational costs, despite its excellent accuracy. Because of this, it may not be suitable for use in urgent clinical settings that demand real-time processing. The method's applicability in clinical workflows could be improved in future studies by enhancing its computational efficiency, which could be achieved through algorithmic refinements or by utilising hardware acceleration techniques.

The narrowness of the dataset utilised for assessment is another restriction. While the 3D-IRCADb dataset is a goldmine for performance benchmarks, the JISTS-FCM method's applicability to other datasets or organs is still up in the air. Furthermore, there is a possibility of diminished robustness in different clinical settings due to the method's sensitivity to parameter tuning. Hence, it would be beneficial for future research to improve the method's adaptability to various segmentation tasks and examine its performance on a broader variety of medical imaging datasets.

A complete list of abbreviations is listed in *Appendix I.*

5.Conclusion and future work

This study introduced a novel and efficient liver segmentation framework using the JISTS-FCM clustering algorithm. The proposed method addresses key challenges in liver segmentation, such as over-segmentation, mis-segmentation, and irregular boundary detection, which are common in conventional FCM-based and deep learning approaches. By integrating the TSO strategy with a similarity-based clustering mechanism and enhanced pre-processing techniques, the proposed model demonstrated superior segmentation accuracy and computational efficiency. The inclusion of the random walker method further refined liver region localization, ensuring consistent and anatomically accurate boundary delineation. Experimental validation on the 3D-IRCADb dataset confirmed that the JISTS-FCM approach significantly outperforms traditional algorithms across multiple evaluation metrics, including DSC, JSC, VOE, RVD, ASSD, RMSD, and MSD. The proposed model achieved a DSC of 97.55% and demonstrated robust performance in terms of sensitivity (96.15%) and specificity (95.75%). Moreover, its lower computational complexity supports its suitability for real-time clinical use. Overall, JISTS-FCM presents a scalable, accurate, and computationally efficient solution for automated liver segmentation. Future research will focus on generalizing the method to other organs and datasets while further improving execution speed and robustness under diverse clinical imaging conditions.

Acknowledgment

None.

Conflicts of interest

The authors have no conflicts of interest to declare.

Data availability

The experimental images used in this study were obtained from the publicly available 3D-IRCADb dataset.

Author's contribution statement

S. Subha: Conceived, designed and implemented the system, collected and analysed data. **U. Kumaran**: Supervision, guided the research direction, and reviewed the manuscript.

References

[1] Saha RS, Roy S, Mukherjee P, Halder RA. An automated liver tumour segmentation and classification model by deep learning based approaches. Computer Methods in Biomechanics and Biomedical Engineering: Imaging & Visualization. 2023; 11(3):638-50.

[2] Li Y, Ou Z, Yu D, He H, Zheng L, Chen J, et al. The trends in death of primary liver cancer caused by specific etiologies worldwide: results from the global burden of disease study 2019 and implications for liver cancer management. BMC Cancer. 2023; 23(1):1-18.

[3] Anwanwan D, Singh SK, Singh S, Saikam V, Singh R. Challenges in liver cancer and possible treatment approaches. Biochimica et Biophysica Acta (BBA)-Reviews on Cancer. 2020; 1873(1):188314.

[4] Dulku G, Dhillon R, Goodwin M, Cheng W, Kontorinis N, Mendelson R. The role of imaging in the surveillance and diagnosis of hepatocellular cancer. Journal of Medical Imaging and Radiation Oncology. 2017; 61(2):171-9.

[5] Krishan A, Mittal D. Ensembled liver cancer detection and classification using CT images. Proceedings of the Institution of Mechanical Engineers, Part H: Journal of Engineering in Medicine. 2021; 235(2):232-44.

[6] Gupta M, Gabriel H, Miller FH. Role of imaging in surveillance and diagnosis of hepatocellular carcinoma. Gastroenterology Clinics. 2018; 47(3):585-602.

[7] Matos AP, Altun E, Ramalho M, Velloni F, Alobaidy M, Semelka RC. An overview of imaging techniques for liver metastases management. Expert Review of Gastroenterology & Hepatology. 2015; 9(12):1561-76.

[8] Goja S, Yadav SK, Yadav A, Piplani T, Rastogi A, Bhangui P, et al. Accuracy of preoperative CT liver volumetry in living donor hepatectomy and its clinical implications. Hepatobiliary Surgery and Nutrition. 2018; 7(3):167-74.

[9] Araújo JD, Da CLB, Ferreira JL, Da SNOP, Silva AC, De PAC, et al. An automatic method for segmentation of liver lesions in computed tomography images using deep neural networks. Expert Systems with Applications. 2021; 180:115064.

[10] Long J, Shelhamer E, Darrell T. Fully convolutional networks for semantic segmentation. In proceedings of the conference on computer vision and pattern recognition 2015 (pp. 3431-40). IEEE.

[11] Hong Y, Mao XW, Hui QL, Ouyang XP, Peng ZY, Kong DX. Automatic liver and tumor segmentation based on deep learning and globally optimized refinement. Applied Mathematics-A Journal of Chinese Universities. 2021; 36(2):304-16.

[12] Alirr OI, Rahni AA. Hepatic vessels segmentation using deep learning and preprocessing enhancement. Journal of Applied Clinical Medical Physics. 2023; 24(5):1-11.

[13] Zhang G, Zhang H, Yao Y, Shen Q. Attention-guided feature extraction and multiscale feature fusion 3D ResNet for automated pulmonary nodule detection. IEEE Access. 2022; 10:61530-43.

[14] Nazir A, Cheema MN, Sheng B, Li P, Kim J, Lee TY. Living donor-recipient pair matching for liver transplant via ternary tree representation with cascade incremental learning. IEEE Transactions on Biomedical Engineering. 2021; 68(8):2540-51.

[15] Aslam MS, Younas M, Sarwar MU, Shah MA, Khan A, Uddin MI, et al. Liver-tumor detection using CNN ResUNet. Computers, Materials & Continua. 2021; 67(2):1899-1914.

[16] Macdonald JA, Zhu Z, Konkel B, Mazurowski MA, Wiggins WF, Bashir MR. Duke liver dataset: a publicly available liver MRI dataset with liver segmentation masks and series labels. Radiology: Artificial Intelligence. 2023; 5(5):1-4.

[17] Zang L, Liang W, Ke H, Chen F, Shen C. Research on liver cancer segmentation method based on PCNN image processing and SE-ResUnet. Scientific Reports. 2023; 13(1):1-14.

[18] Zhou HY, Guo J, Zhang Y, Han X, Yu L, Wang L, et al. nnFormer: volumetric medical image segmentation via a 3D transformer. IEEE Transactions on Image Processing. 2023; 32:4036-45.

[19] Riana D, Na'am J, Saputri DU, Hadianti S, Aziz F, Liawatimena SP, et al. Comparison of segmentation analysis in nucleus detection with GLCM features using OTSU and polynomial methods. Jurnal Rekayasa Sistem Dan Teknologi Informasi. 2023; 7(6):1422-9.

[20] Jamali A, Rostamy-malkhalifeh M, Kargar R. The novel self-organizing map combined with fuzzy C-means and K-means convolution for a soft and hard natural digital image segmentation. AUT Journal of Mathematics and Computing. 2024; 5(2):151-65.

[21] Budak Ü, Guo Y, Tanyildizi E, Şengür A. Cascaded deep convolutional encoder-decoder neural networks for efficient liver tumor segmentation. Medical Hypotheses. 2020; 134:109431.

[22] Li Y, Zhao YQ, Zhang F, Liao M, Yu LL, Chen BF, et al. Liver segmentation from abdominal CT volumes based on level set and sparse shape composition. Computer Methods and Programs in Biomedicine. 2020; 195:105533.

[23] Alalwan N, Abozeid A, Elhabshy AA, Alzahrani A. Efficient 3D deep learning model for medical image

semantic segmentation. Alexandria Engineering Journal. 2021; 60(1):1231-9.
[24] Aghamohammadi A, Ranjbarzadeh R, Naiemi F, Mogharrebi M, Dorosti S, Bendechache M. TPCNN: two-path convolutional neural network for tumor and liver segmentation in CT images using a novel encoding approach. Expert Systems with Applications. 2021; 183:115406.
[25] Ahmad M, Qadri SF, Qadri S, Saeed IA, Zareen SS, Iqbal Z, et al. A lightweight convolutional neural network model for liver segmentation in medical diagnosis. Computational Intelligence and Neuroscience. 2022; 2022(1):1-16.
[26] Fan T, Wang G, Li Y, Wang H. Ma-net: a multi-scale attention network for liver and tumor segmentation. IEEE Access. 2020; 8:179656-65.
[27] Alirr OI. Deep learning and level set approach for liver and tumor segmentation from CT scans. Journal of Applied Clinical Medical Physics. 2020; 21(10):200-9.
[28] Tang W, Zou D, Yang S, Shi J, Dan J, Song G. A two-stage approach for automatic liver segmentation with Faster R-CNN and DeepLab. Neural Computing and Applications. 2020; 32:6769-78.
[29] Rahman H, Bukht TF, Imran A, Tariq J, Tu S, Alzahrani A. A deep learning approach for liver and tumor segmentation in CT images using ResUNet. Bioengineering. 2022; 9(8):1-19.
[30] Kushnure DT, Talbar SN. MS-UNet: a multi-scale UNet with feature recalibration approach for automatic liver and tumor segmentation in CT images. Computerized Medical Imaging and Graphics. 2021; 89:101885.
[31] Winkel DJ, Weikert TJ, Breit HC, Chabin G, Gibson E, Heye TJ, et al. Validation of a fully automated liver segmentation algorithm using multi-scale deep reinforcement learning and comparison versus manual segmentation. European Journal of Radiology. 2020; 126:108918.
[32] Almotairi S, Kareem G, Aouf M, Almutairi B, Salem MA. Liver tumor segmentation in CT scans using modified SegNet. Sensors. 2020; 20(5):1-13.
[33] Tang X, Jafargholi RE, Coudyzer W, Bertels J, Robben D, Schramm G, et al. Whole liver segmentation based on deep learning and manual adjustment for clinical use in SIRT. European Journal of Nuclear Medicine and Molecular Imaging. 2020; 47:2742-52.
[34] Ranjbarzadeh R, Saadi SB. Automated liver and tumor segmentation based on concave and convex points using fuzzy c-means and mean shift clustering. Measurement. 2020; 150:107086.
[35] Lei T, Wang R, Zhang Y, Wan Y, Liu C, Nandi AK. DefED-Net: deformable encoder-decoder network for liver and liver tumor segmentation. IEEE Transactions on Radiation and Plasma Medical Sciences. 2021; 6(1):68-78.
[36] Ranjbarzadeh R, Jafarzadeh GS, Bendechache M, Amirabadi A, Ab RMN, Baseri SS, et al. Lung infection segmentation for covid-19 pneumonia based on a cascade convolutional network from CT images. BioMed Research International. 2021; 2021(1):1-16.
[37] Xie L, Han T, Zhou H, Zhang ZR, Han B, Tang A. Tuna swarm optimization: a novel swarm-based metaheuristic algorithm for global optimization. Computational Intelligence and Neuroscience. 2021; 2021(1):1-22.
[38] Tuerxun W, Xu C, Guo H, Guo L, Zeng N, Cheng Z. An ultra-short-term wind speed prediction model using LSTM based on modified tuna swarm optimization and successive variational mode decomposition. Energy Science & Engineering. 2022; 10(8):3001-22.
[39] Drees D, Eilers F, Jiang X. Hierarchical random walker segmentation for large volumetric biomedical images. IEEE Transactions on Image Processing. 2022; 31:4431-46.
[40] Manjunath RV, Kwadiki K. Modified U-NET on CT images for automatic segmentation of liver and its tumor. Biomedical Engineering Advances. 2022; 4:1-5.
[41] Rodríguez M, Alonso-alonso R, Borregón J, Díaz-alejo JF, Manso-alonso R, Rebollo-González M, et al. Molecular identity revealed by nanostring analysis between tumoral erythroderma and inflammatory erythroderma. European Journal of Cancer. 2023; 190.
[42] Moghbel M, Mashohor S, Mahmud R, Saripan MI. Automatic liver segmentation on computed tomography using random walkers for treatment planning. EXCLI Journal. 2016; 15:500-17.
[43] Ma J, Deng Y, Ma Z, Mao K, Chen Y. A liver segmentation method based on the fusion of VNet and WGAN. Computational and Mathematical Methods in Medicine. 2021; 2021(1):1-12.
[44] Maqsood M, Bukhari M, Ali Z, Gillani S, Mehmood I, Rho S, et al. A residual-learning-based multi-scale parallel-convolutions-assisted efficient CAD system for liver tumor detection. Mathematics. 2021; 9(10):1-15.
[45] Chartrand G, Cresson T, Chav R, Gotra A, Tang A, De GJA. Liver segmentation on CT and MR using Laplacian mesh optimization. IEEE Transactions on Biomedical Engineering. 2016; 64(9):2110-21.
[46] Sun C, Guo S, Zhang H, Li J, Chen M, Ma S, et al. Automatic segmentation of liver tumors from multiphase contrast-enhanced CT images based on FCNs. Artificial Intelligence in Medicine. 2017; 83:58-66.

S. Subha is currently an Assistant Lecturer in the Department of Computer Applications at Arunachala Arts and Science College. She earned her Bachelor of Computer Applications (BCA) from Noorul Islam Arts and Science College, affiliated with Manonmaniam Sundaranar University, in 2014, and her Master of Computer Applications (MCA) from St. Xavier's Engineering College under Anna University in 2016. Her research interests include Digital

Image Processing. Since 2019, she has been serving as an Assistant Lecturer in Computer Applications and is currently pursuing her Ph.D. in Computer Applications at Noorul Islam University, Kumaracoil, Kanyakumari.
Email:subhasundar93@gmail.com

Dr. U. Kumaran is currently working as an Associate Professor at Saveetha Engineering College, Chennai. He holds a Bachelor's degree in Computer Science and Engineering from Madurai Kamaraj University, and a Master's degree in the same field from Anna University, Trichy. He earned his Doctoral degree from Noorul Islam Centre for Higher Education, Kumaracoil, Kanyakumari District, Tamil Nadu. Previously, he served as Deputy Director at the Centre for Advanced Computing and Robotics, Noorul Islam University, Kumaracoil. With over 25 years of teaching experience across various colleges and universities, he has published more than 20 research papers in reputed journals and conferences. His areas of interest include Vehicular Ad Hoc Networks, Cloud Computing, and Image Processing.
Email: kumaranu@saveetha.ac.in

Appendix I

S. No.	Abbreviation	Description
1	3D	3 Dimensional
2	AI	Artificial Intelligence
3	ASSD	Average Symmetric Surface Distance
4	AUC	Area Under the Curve
5	CCLAHE	Covarianced Contrast Limited Adaptive Histogram Equalization
6	CCP	Concave and Convex Point
7	CNN	Convolutional Neural Network
8	CSA	Cuckoo Search Algorithm
9	CT	Computed Tomography
10	DefED-Net	Deformable Encoder-Decoder Network
11	DS-Conv	Depth-Separable Convolution
12	DSC	Dice Similarity Coefficient
13	DSL	Deep Supervised Learning
14	EDCNN	Deep Convolutional Encoder-Decoder Neural Network
15	EPMF	Edge Preserved Median Filter
16	FCM	Fuzzy C-Means
17	FCN	Fully Convolutional Network
18	FCNN	Fully Convolutional Neural Network
19	FP	False Positive
20	Ga-CNN	Gaussian-Weight Initialization of Convolutional Neural Network
21	GLCM	Gray Level Co-occurrence Matrix
22	GPU	Graphics Processing Unit
23	JISTS-FCM	Jaccard with Interpolation Scaled Tuna Swarm-Based Fuzzy C-Means
24	JSC	Jaccard Similarity Coefficient
25	LDOG	Local Direction of Gradient
26	LiTS	Liver Tumor Segmentation
27	LMO	Laplacian Mesh Optimization
28	LTP	Local Tetra Pattern
29	Ma-Net	Multi-scale Attention Net
30	MC-FCN	Multi-Constraint Fully Convolutional Network
31	MFAB	Multi-scale Fusion Attention Block
32	MPC	Multi-Scale Parallel Convolution Blocks
33	MRI	Magnetic Resonance Imaging
34	MSD	Maximum Symmetric Surface Distance
35	PAB	Position-wise Attention Block
36	RCNN	Region based Convolutional Neural Network
37	RMSSD	Root Mean Square Symmetric Surface Distance
38	ROC	Receiver Operating Characteristic
39	ROI	Regions of Interest
40	RVD	Relative Volume Difference
41	SIRT	Selective Internal Radiation Therapy
42	SSC	Sparse Shape Composition
43	TP	True Positive
44	TSO	Tuna Swarm Optimization
45	TSO-FCM	Tuna Swarm Optimization Algorithm-Fuzzy C-means
46	VOE	Volumetric Overlap Error